Comparative study of nano-ZSM-5 catalysts synthesized in OH^- and F^- medium

Zhengxing Qin,[a] Louwanda Lakiss,[a] Lubomira Tosheva,[b] Jean-Pierre Gilson,[a] Aurelie Vicente,[a] Christian Fernandez,[a] Valentin Valtchev[a*]

[a] *Laboratoire Catalyse & Spectrochimie, ENSICAEN - Université de Caen – CNRS, 6 boulevard du Maréchal Juin, 14050 Caen, France*
[b] *Division of Chemistry and Environmental Science, Manchester Metropolitan University, Chester St., Manchester M1 5GD, United Kingdom*

Abstract

This study reports on the seeded synthesis of MFI-type (ZSM-5) zeolite in fluoride medium at pH=8.5. Crystal growth kinetics of the material as a function of the seed content and crystallization temperature was studied. The crystallization time was reduced to 1.5 h and crystals with sizes below 200 nm and a Si/Al ratio of 23.6 were obtained. Material with similar characteristics synthesized in hydroxyl medium (ZSM-5-OH) was used for the comparative study of zeolites synthesized in different crystallization medium. The physicochemical properties of ZSM-5-F and ZSM-5-OH were compared and particular attention was paid to the nature, number and distribution of active sites. The set of experimental data showed that the two zeolites exhibited similar number of Brønsted acid sites, however the material synthesized in hydroxyl medium contained substantially larger number of surface and internal silanols that had strong impact on its catalytic properties. The two materials exhibited similar selectivity in methanol transformations. However, the material synthesized in flouride medium showed superior performance in terms of activity and deactivation. The obtained data showed that seeded synthesis in fluoride medium can be used for the preparation of superior zeolite catalysts.

Keywords: zeolite synthesis, fluoride medium, nanocrystals, methanol conversion

1 Introduction

Microporous zeolite-type materials have already been used in industry for half a century.[1] Their catalytic and separation properties are exploited in some of the largest chemical processes, for instance in the oil refining and petrochemicals production.[2] Despite their industrial application, their properties / synthetic procedures continue to be improved in order to meet current environmental and technological challenges. Two approaches have been used to tune the zeolite characteristics. There has been an intense research in the development of post-synthesis modification methods to tailor the properties of pre-made crystals.[3] Nevertheless, in situ control of the zeolite intrinsic characteristics remains indispensable for the industrial preparation of zeolites.

The physicochemical properties of zeolites are a function of the chemical composition of the initial gel or solution and the crystallization conditions used for their synthesis. The silica source plays a particularly important role in the crystallization process.[4] Further, the structure-directing and mineralizing agents determine the course of the reaction and the structure type to be formed.[5] Alkali metal cation – water complexes and positively charged organic molecules are the most often used structure-directing agents (SDA). The role of the mineralizer is to convert the initial reactants into reactive forms and transport them to SDA. After completion of the reaction, the mineralizing agent is released and available to take part in a new cycle. Consequently, the role of the mineralizer is often compared to that of a catalyst. The most common mineralizer for silica and aluminosilicate-based zeolites is the hydroxyl (OH^-) ion. Fluoride (F^-) ions are also used in zeolite synthesis.[6,7] There are, however, fundamental differences in the zeolite formation in alkaline and fluoride medium.[8] Fluoride ions are mineralizing agents in the synthesis of high silica zeolites. The syntheses in fluoride medium are performed at relatively low pH (< 10). Such conditions lead to several important consequences: (i) the growth at close to neutral pH minimizes the number of non-

bridging ≡SiO- defects; and (ii) the supersaturation of the framework-forming species is lower than that in an OH^- medium. Thus, the crystals synthesized in fluoride medium comprise less framework defects, which have a positive impact on their catalytic, sorption, hydrophobic and thermal properties. On the other hand, crystals synthesized under such conditions are relatively large imposing serious diffusion limitations and leading to pore blocking and coke formation.

The exact role of the fluoride ions in the zeolite synthesis has been discussed in a number of studies. Besides mineralizer, F^- has specific functions in the zeolite framework. Solid-state nuclear magnetic resonance (NMR) and single crystal X-ray diffraction (XRD) studies have been performed in order to locate the fluoride ions in as-made silicalite-1 (MFI-type) crystals.[9,10] Both methods found that F^- counter anions were present in the $[4^15^26^2]$ units of the MFI-type structure. XRD analysis revealed the presence of five coordinated Si atoms in the zeolite framework, located in slightly distorted trigonal bipyramid built of four framework oxygen atoms and a fluoride anion.[10] Pentacoordinated silicon units have been found in other zeolites (Beta, SSZ-23, ITQ-3, ITQ-4, ZSM-12) synthesized in fluoride medium.[11] Theoretical studies have also been performed in order to elucidate the interactions between F^- and positively charged organic cations employed in the synthesis of a series of zeolite structures, IFR, ITH, IWR, STF and STT.[12] It was proposed that during the initial stages of zeolite structure formation the location of the F^- anion is governed by the long-range forces that determine in which cage it will be located, then the F^- form a covalent bond with Si to form the pentacoordinated units. Besides a counter anion of SDA cation, the fluoride anion can also play a structure-directing role. It has been proven that F^- is able to form double four member ring (D4R) units and thus to direct the zeolite formation.[13] The co-structure-directing ability of F^- and Ge^{4+} was used by Corma and co-workers in the synthesis of extra-large pore Ge-silicate molecular sieves.[14]

Indeed, F^- as mineralizing agent offers certain advantages, especially when the goal is the synthesis of new framework topologies or to extend existing framework compositions to high- or all-silica members of a particular framework type. High quality large crystals synthesized in fluoride medium are very useful for the fundamental studies of zeolites. However, the fluoride medium synthesis brings certain disadvantages in the zeolite preparation. As mentioned, lower nucleation rate in fluoride systems leads to larger ultimate crystals. Although almost defect-free, such crystals are not appropriate for catalytic and separation processes because of long diffusion paths. Ivanova et al. have employed methanol conversion as a test reaction to compare the catalytic performance of 30-50 μm ZSM-5 crystals synthesized in fluoride medium with 2-3 μm ZSM-5 crystals synthesized in hydroxyl medium.[15] The larger crystals showed similar catalytic performance. However, in order to accurately evaluate the performance of zeolites prepared in the two types of media, crystals with similar crystal sizes and compositions have to be compared. It should also be mentioned that if the major drawback of the synthesis in fluoride medium, namely the large crystals size, is not circumvented, the exceptional physicochemical properties of zeolite crystals synthesized under such conditions could not be utilized.

The primary goal of this study was to optimize the synthesis of ZSM-5 crystals in fluoride medium. Silicalite-1 nanocrystals were employed as seeds in order to accelerate the crystallization process and provide very small crystallites. Amongst the objectives was also to conduct a comparative study of the physicochemical properties of similar in size zeolite crystals synthesized in fluoride and hydroxyl medium. Finally, the materials were subjected to catalytic tests in order to evaluate their potential as heterogeneous catalysts. Methanol-to-hydrocarbons (MTH) conversion, which provides valuable information of the structure-specific performance of a zeolite catalyst, was employed as a test reaction.[16]

2 Results and discussion

2.1 Synthesis of initial materials

The use of nanosized seeds have been found to accelerate the crystallization rate leading to substantial reduction of the ultimate crystal size of zeolites.[17] Hence, nanosized silicalite-1 crystals with an average size of 80 nm and narrow particle size distribution were used to control the formation of ZSM-5 in fluoride medium.

2.1.1 Synthesis in fluoride medium: effect of F^- on ZSM-5 formation

Initially, experiments to study the effect of fluoride species on ZSM-5 formation were performed. Our preliminary results showed that the system 0.142TPABr : 0.135TPAOH : $0.072Al_2O_3$: $1.0SiO_2$: $0.616NH_4F$: $20H_2O$ comprising 5 wt. % seeds yielded high quality ZSM-5 at 423 K. This system was also employed without the addition of NH_4F and subjected to hydrothermal treatment at 423 K. The pH of the system was adjusted to 10.5 by addition of diluted HCl, which corresponded to the pH value of the gel when ammonium fluoride was used in the synthesis. This gel was hydrothermally treated, but the material obtained was still amorphous after one month of treatment. It should be mentioned that when NH_4F was used in zeolite synthesis, the pH of the gel was adjusted to 8.5 (see EXPERIMENTAL). Nevertheless, a gel with similar composition yielded highly crystalline ZSM-5 within 3.5 h. This is a sound proof of the impact of F^- on zeolite formation. In order to verify this, the crystallization of the gel that remained amorphous after hydrothermal treatment for one month was interrupted and the usual amount of NH_4F was added. After 56 h of treatment at 373 K, crystallization was completed and highly crystalline ZSM-5 (XRD pattern not shown) was obtained. The set of experimental data unambiguously confirmed that in this pH range, fluoride anions induce a very rapid growth of the seed crystals.

As discussed in the introduction, the F^- anions in the zeolite structure occupy specific positions minimizing the number of non-bridging ≡SiO- defects.[9] We have subjected a highly

crystalline ZSM-5 sample to ^{19}F MAS NMR study and the spectrum obtained is shown in Figure 1. The spectrum exhibits a signal at -64 ppm along with a weaker one at -120 ppm. The peak at -64 ppm is assigned to F^- in a $[4^15^26^2]$ cage,[10] while the signal at -120 ppm is most probably due to the presence of free fluoride anions.[18,19] The peak at about -116 ppm is typical of F^- ions in aqueous NH_4F solutions. In our case, this peak can be attributed to F^- counter ion of NH_4^+ or tetrapropylammonium cation in the zeolite channels. Hence, less non-bridging ≡SiO- defects can be expected to present in samples synthesized in fluoride medium.

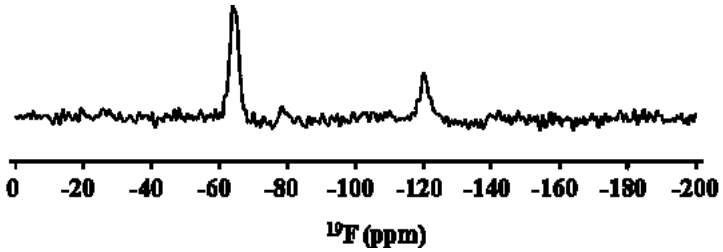

Figure 1. ^{19}F MAS NMR spectrum of highly crystalline ZSM-5 sample synthesized in F^- medium in the presence of 5 wt. % seeds.

2.1.2 Synthesis in fluoride medium: effect of the amount of seeds

A series of experiments was performed at 423 K with gels containing 0, 2.5 and 5 wt.% silicalite-1 seeds. Error! Reference source not found. represents the crystal growth curves of these three systems. As can be seen, the induction period depended drastically on the amount of seeds added. The induction period in the absence of seeds was about 20 h. First traces of crystalline material were observed after 25 h and the mass transformation of amorphous material into ZSM-5 took place between 30 and 45 h crystallization time. The extension of the crystallization time to 65 h did not change substantially the X-ray crystallinity of the material (**Figure SI1**).

The addition of 2.5 wt.% silicalite-1 seeds into the initial gel accelerated the crystallization

rate. Crystalline material was observed after 5 h of treatment and fully crystalline ZSM-5 was obtained after 17 h (**Figure SI2**). The crystallization of ZSM-5 zeolite in the presence of 5 wt.% silicalite-1 seeds was much faster. Crystalline MFI-type material was detected after 1 h of treatment and the crystallization was completed within 3.5 h (**Figure SI3**).

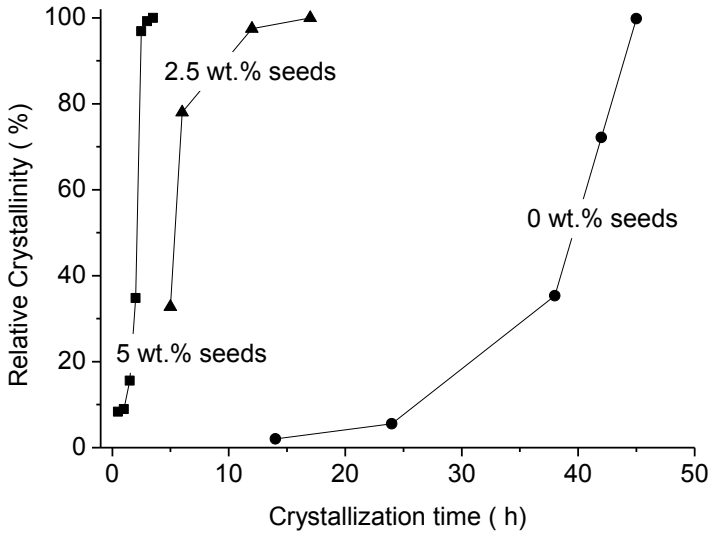

Figure 2. ZSM-5 crystal growth kinetics curves at 423 K from seed-free gels and gels containing 2.5 and 5 wt. % silicalite-1 seeds.

The SEM inspection of the materails prepared in the absence and in the presence of seeds showed the formation of uniform crystals in all samples. Their size, however, was different and the largest crystals were observed in the product obtained without using seeds. The crystals were about 3 μm in size with the typical of ZSM-5 coffin shape morphology (**Figure 3A)**. Sub-micrometer crystals were obseved in the sample synthesized with 2.5 wt. % seeds. The morphology of the crystals was similar to that of a non-seeded sample, i.e., coffin shape crystals with well developed crystal faces (**Figure 3B**). Further increase of the seed content (5 wt. %) ressulted in much smaller, ca. 200 nm ZSM-5 crystals (**Figure 3C**). Again well shaped crystals were formed, but in this case they were almost isometric and the twin crystals were less developed. Additional synthesis using 10 wt. % seeds (XRD pattern not shown) was performed in order to prepare even smaller zeolite nanocrystals. However, dramatic changes

in the morphology and the size of the crystalline product were not observed (**Figure 3D**). The crystallites were slightly smaller (ca. 150 nm) with morphological features very close to the product synthesized with 5 wt. % seeds.

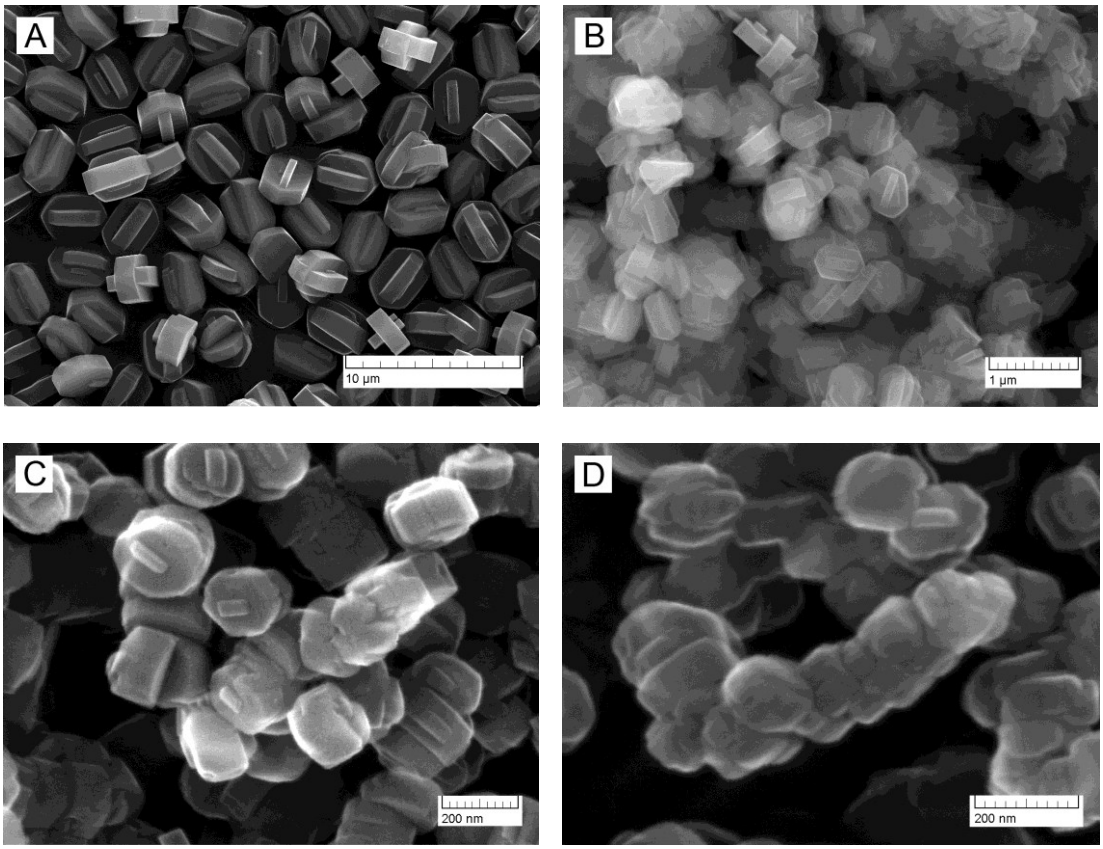

Figure 3. SEM micrographs of the ZSM-5 crystals synthesized in F^- medium (A) in the absence of seeds and in the presence of (B) 2.5wt.%, (C) 5 wt.% and (D) 10 wt. % seeds.

2.1.3 Synthesis in fluoride medium: effect of temperature

The initial gel containing 5 wt. % seeds yielded relatively small ZSM-5 crystals for a short period of time. This system was employed to study the effect of crystallization temperature on the crystal growth rate and crystal size. Additional experiments were performed at 443 K (**Figure SI4**) and 403 K (**Figure SI5**) and the results were compared with those obtained at 423 K. As expected, the crystallization rate increased with crystallization temperature,

whereas much longer crystallization time was needed to obtain highly crystalline product at 403 K (**Figure 4**). At 443 K, crystallization was completed after 1.5 h. Usually, the increase of the crystallization temperature results in larger zeolite crystals. However, the size of the crystals synthesized at 443 K (**Figure 5A**) did not differ from those synthesized at 423 K (**Figure 2C**). This result suggests that the crystallization process in the system is governed by the seeds, i.e., the amount of seeds control the ultimate crystal size. Again, coffin-like crystals with size of about 200 nm were synthesized. The result at lower crystallization temperature (403 K) was fairly different. The induction period was long; the crystallization started after 40 h and was completed within 72 h (**Figure 4**). The morphology of the crystals synthesized was also substantially different. Instead of the well-shaped crystals synthesized at 423 K and 443 K, aggregates built of smaller crystallites were observed (**Figure 5B**). The size of the aggregates ranged between 250 and 400 nm. These differences in the size and morphology can be related to the zeolite crystallization mechanism, which was strongly influenced by the crystallization temperature. At 443 K, there was no induction period, which suggested that only the seeds introduced into the system grew to become crystals. There was not an induction period at 423 K, meaning that at higher temperature the seeds started to grow immediately. In contrast, a long induction period was observed at 403 K. The latter is a strong evidence for reorganization in the system similar to zeolite yielding systems free of seeds. New viable nuclei are formed and continue to grow alongside the seeds into zeolite crystals. The formation of aggregates with complex morphology built up of much smaller crystals strongly supports this conclusion.

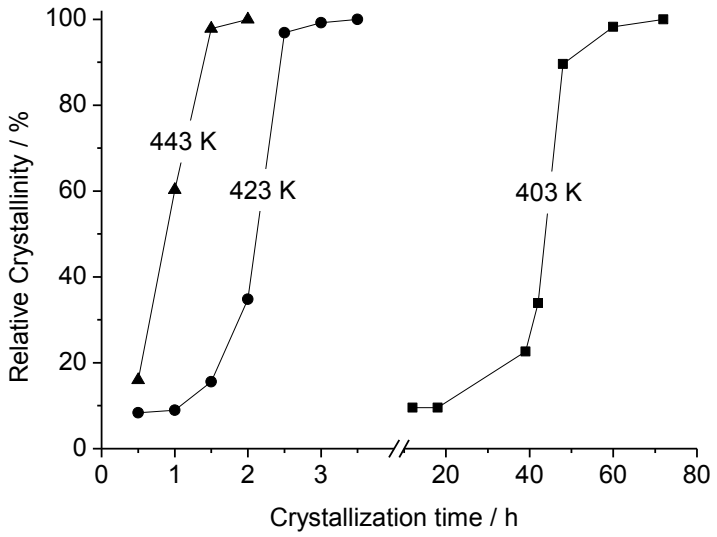

Figure 4. Crystal growth curves of ZSM-5 synthesized at different temperatures from gels containing 5 wt % seeds.

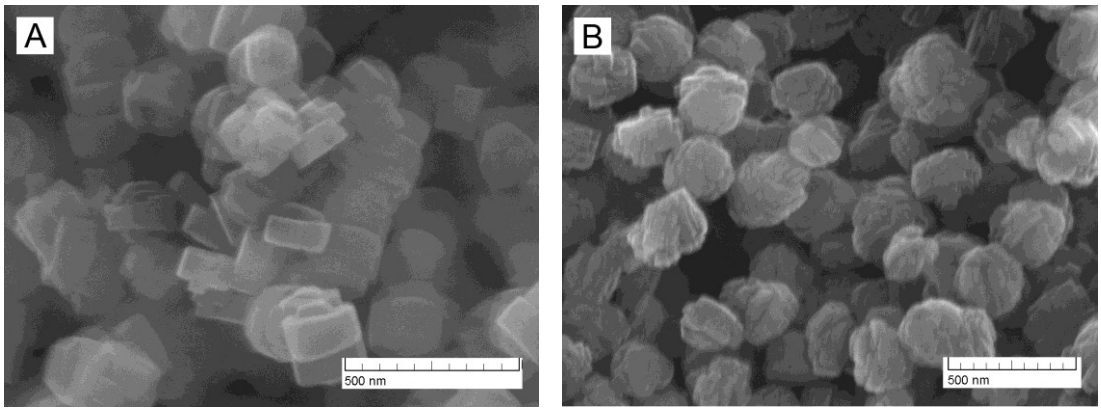

Figure 5. SEM micrographs of ZSM-5 crystals synthesized in fluoride medium with 5 wt. % seeds at (A) 443 K and (B) 403 K.

2.1.4 Synthesis of nano-ZSM-5 in OH^- medium

Highly crystalline ZSM-5 materials was synthesized in an OH^- medium (Error! Reference

source not found. **SI6**). No indications of the presence of other crystalline phases or amorphous material were found. SEM inspection showed that the solid compred complex aggrates of different size and random morphology (**Figure 6A**). High magnification micrographs showed that the aggregates were built of nanocrystallites with size of ca. 50 nm (**Figure 6B**).

The physicochemical properties of this sample were compared with ZSM-5 synthesized in fluoride medium at 403 K for 65 h from a gel containg 5 wt % seeds (**Figure 5B**).

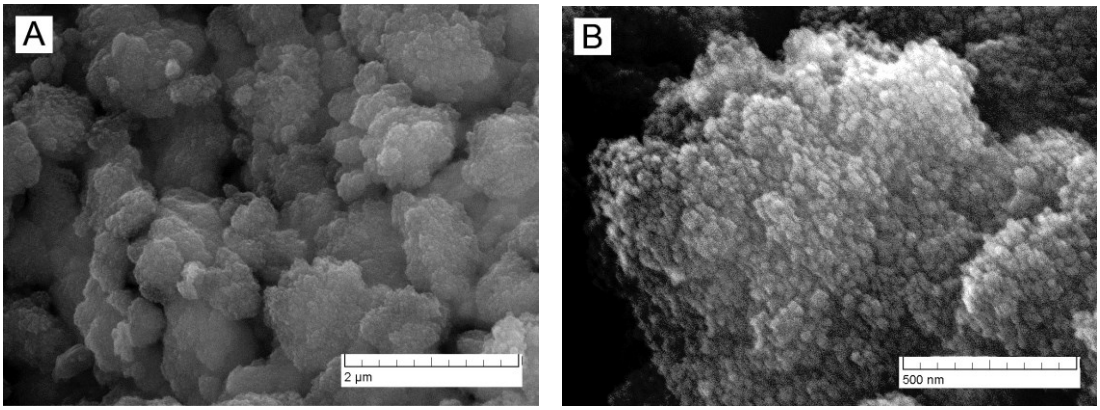

Figure 6. (A) Low and (B) high magnification SEM micrographs of ZSM-5 crystals synthesized in hydroxyl medium.

2.2 Comparative study of the physicochemical properties of nano ZSM-5 crystals synthesized in F^- and OH^- medium

Both fluoride and hydroxyl medium syntheses provided nanosized crystals. According to the SEM study, the crystals synthesized in highly alkaline media were three to four times smaller with respect to their neutral-medium synthesized counterparts.

The chemical analysis of the two samples showed similar Si/Al ratio, which was 23.6 and 24.4 for the materails synthesized in fluoride (ZSM-5-F) and hydroxyl (ZSM-5-OH) medium, respectively. These values correspond to incorporation of four TPA cations in a

unit cell, which gives Si/Al~24. This result is consistent with the synthesis conditions employed, where alkali metal cations were not used.

The nitrogen adsorption/desorption isotherms of the two samples were very similar (**Figure 7**). Both isotherms were indicative of the presence of micropores evident from the steep increase in the gas adsorbed at low relative pressures, and mesopores judged by the hysteresis loops in the isotherms. This result is not surprising considering the similar crystallinity and morphology of the two samples. There were differences in the mesopore size distribution as seen by the shape of the isotherms and the BJH pore size distributions (**Figure 7, Inset**). The ZSM-5-F sample showed sharper pore size distribution in the range 2.5 – 15 nm, which may be due to the narrower crystal size distribution of this sample (**Figure 5B**). Nevertheless, the BET and external surface areas as well as the micro- and mesopore volumes determined from gas adsorption (Table 1) were similar for the two samples.

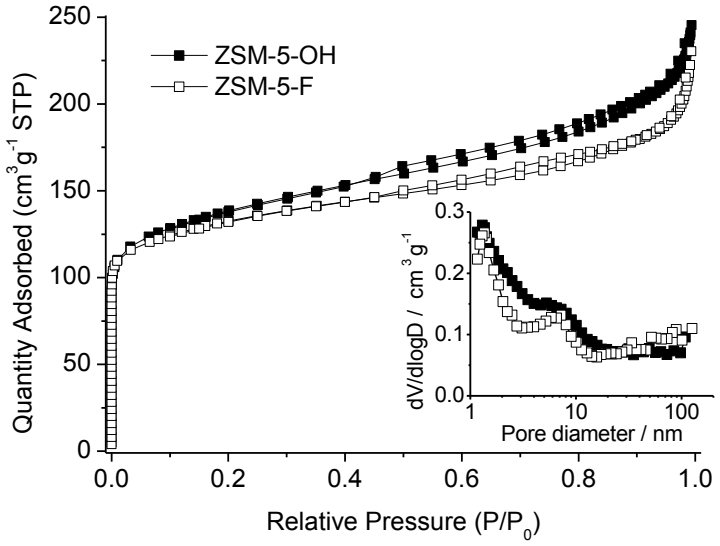

Figure 7. Nitrogen adsorption/desorption isotherms of nano ZSM-5 synthesized in OH^- and F^- medium. Inset: BJH pore size distribution (adsorption branches) of the mesopores in the two samples.

Table 1. Specific surface area and porosity characteristics of nano ZSM-5 crystals synthesized OH^- and F^- medium.

Samples	S_{BET}	V_{mic}	S_{ext}	V_{meso}
	$m^2\ g^{-1}$	$cm^3\ g^{-1}$	$m^2\ g^{-1}$	$cm^3\ g^{-1}$
ZSM-5-OH	462	0.217	69	0.15
ZSM-5-F	438	0.206	53	0.13

Since the ultimate goal of the study was the evaluation of the catalytic properties of ZSM-5 synthesized in OH^- and F^- medium, the number of Brønsted and Lewis sites and different silanols in the two samples was of particular importance. Hence, a ^1H MAS NMR was performed on samples dehydrated at 450 °C using a home-made device.[20] Proton MAS NMR spectra are shown in **Figure 8** along with a Gaussian decomposition. Four main resonances were observed in each sample. The resonance at 1.7 ppm is attributed to external silanol groups, while the one at 2.3 ppm can be attributed to silanol groups in defect sites. The peak around 2.6 ppm is typical of H linked to extra-framework aluminum. Finally, the one at about 3.8 ppm corresponds to Brønsted acidic sites. In order to quantify the different proton site concentrations, a signal intensity calibration was performed using a known amount of protons in adamantane sample. All data obtained are reported in **Table 2**. In agreement with previous studies, a lower amount of silanol nests was determined for the sample prepared in fluoride medium.[21] There is also a substantial difference in the surface silanols between ZSM-5-F and ZSM-5-OH samples. Themaller crystals synthesized in hydroxyl medium possessed much larger (factor of three) numbers of surface silanols. Protons connected to extra-framework aluminium species were found in two samples. The

peak was more intense in the spectrum of ZSM-5-F.

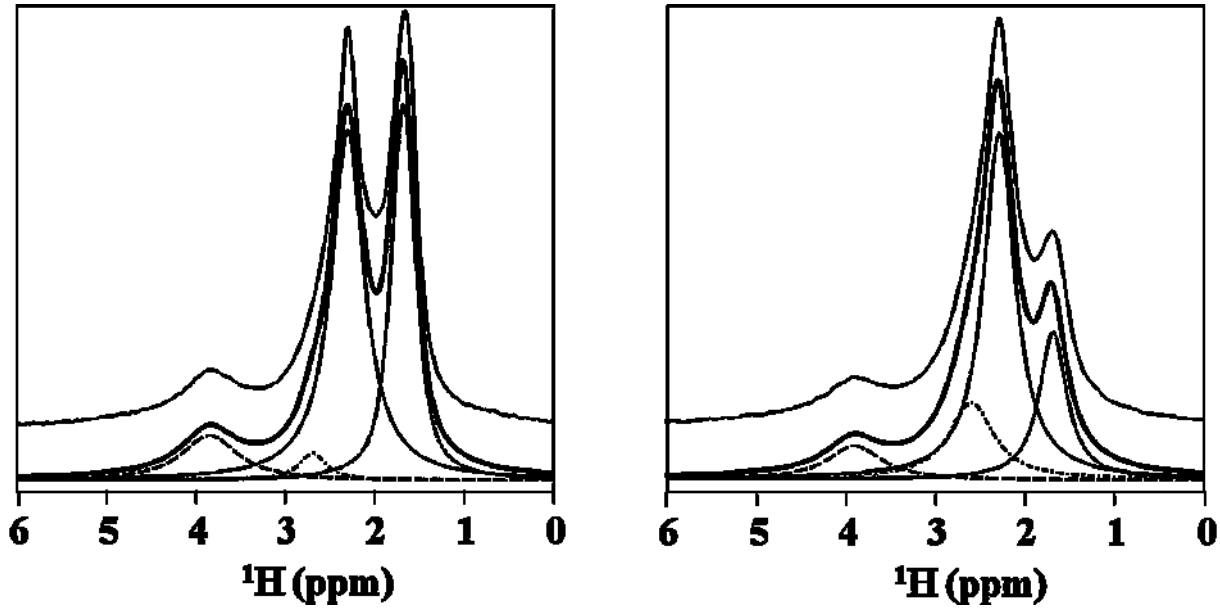

Figure 8. ^{1}H MAS NMR spectra of (A) ZSM-5-OH and (B) ZSM-5-F with decomposition of the different peaks.

Table 2. ^{1}H MAS NMR shifts, assignments and intensity of OH groups in dehydrated ZSM-5-OH and ZSM-5-F samples.

Sample	**SiOH $_{ext.}$**		**SiOH $_{def.}$**	
	d/ppm	μmol/g	d/ppm	μmol/g
ZSM-5-OH	1.7	1700	2.3	2364
ZSM-5-F	1.7	678	2.3	1818

^{27}Al MAS NMR spectra of ZSM-5 prepared in OH- and F- medium are presented in **Figure 9A**. Two resonances with approximately the same intensities were observed in the spectra. The first one at 55 ppm is attributed to tetrahedral coordinated Al, which reflects

Al in the framework. The second at 0 ppm corresponds to hexacoordinated extra-framework Al atoms. Thus, the two samples comprise similar aluminum species as the major part of aluminium is in framework positions.

Figure 9B shows the ^{29}Si MAS NMR spectra of hydroxyl and fluoride medium-synthesized samples. A main peak is observed at -112.8 ppm with a shoulder at -116.0 ppm. Both peaks correspond to tetrahedral Si-O-Si (SiOAl) environment. An additional peak is observed at 105.7 ppm, which can be assigned to tetrahedral Si(1Al) framework. From the intensity of these resonances the Si/Al ratio is estimated to be 27 for both samples.[22] This value is slightly higher but still consistent with the chemical analysis and confirms that the Al content in the two zeolites is similar.

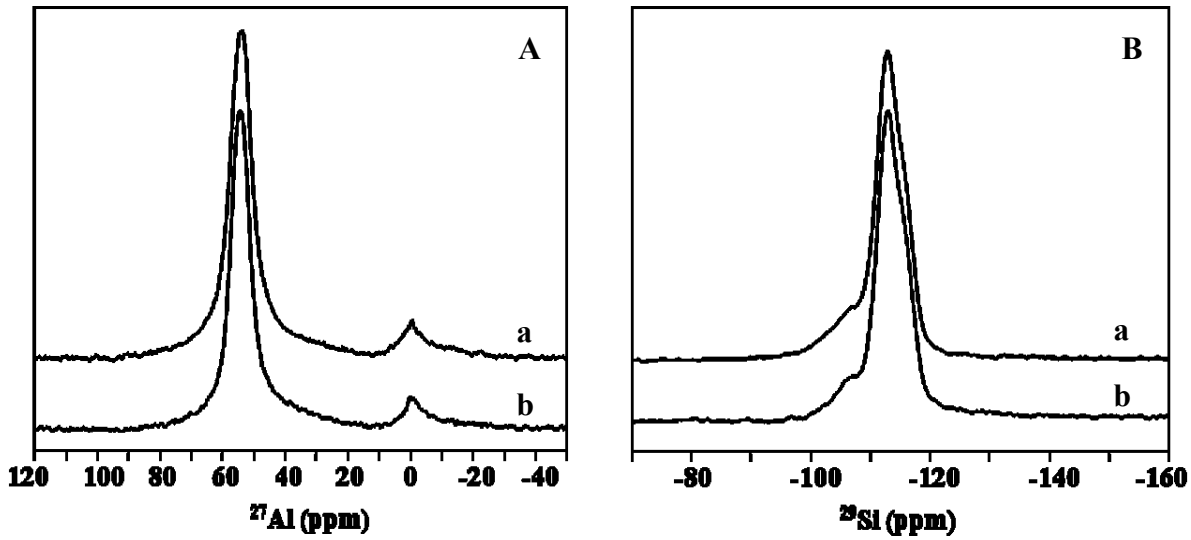

Figure 9. (A) ^{27}Al MAS NMR spectra of (a) ZSM-5-OHand (b) ZSM-5-F; and (B) ^{29}Si MAS NMR spectra of (a) ZSM-5-OH and (b) ZSM-5-F.

The NMR analysis of the active sites in two catalysts was complemented by an IR study. The infrared spectra of ZSM-5-OH and ZSM-5-F samples after activation are presented in **Figure 10**. Two major bands are observed in the OH-stretch vibrations region. The first one at 3610 cm^{-1} corresponds to Brønsted acid sites and the second one located at 3745 cm^{-1} is attributed to internal and surface silanols. The latter can be decomposed into three main bands at 3745

cm^{-1}, 3735 cm^{-1}, 3726 cm^{-1}, and a small broad band at 3700 cm^{-1}. According to the literature, the band at 3745 cm^{-1} is assigned to external silanol sites while the one at 3726 cm^{-1} corresponds to the silanol sites present in the micropores.[23] In addition, a smaller band appears at 3666 cm^{-1}, which is usually attributed to Lewis acid sites that could be extra-framework aluminium connected to the zeolite structure.[24] It should be noted that the band at 3500 cm^{-1}, which is generally assigned to silanol nests, is not clearly observed due to the activation conditions (823K). Although the two samples exhibit similar Brønsted sites, they display different silanol contents. As seen from the inset in **Figure 10**, the band at 3745 cm^{-1} with the shoulder at 3726 cm^{-1} is more intense in the hydroxyl medium-synthesized sample. This means that ZSM-5-OH displays not only more external silanol sites due to the smaller crystallites, but also more internal silanol sites. In order to estimate the amount of

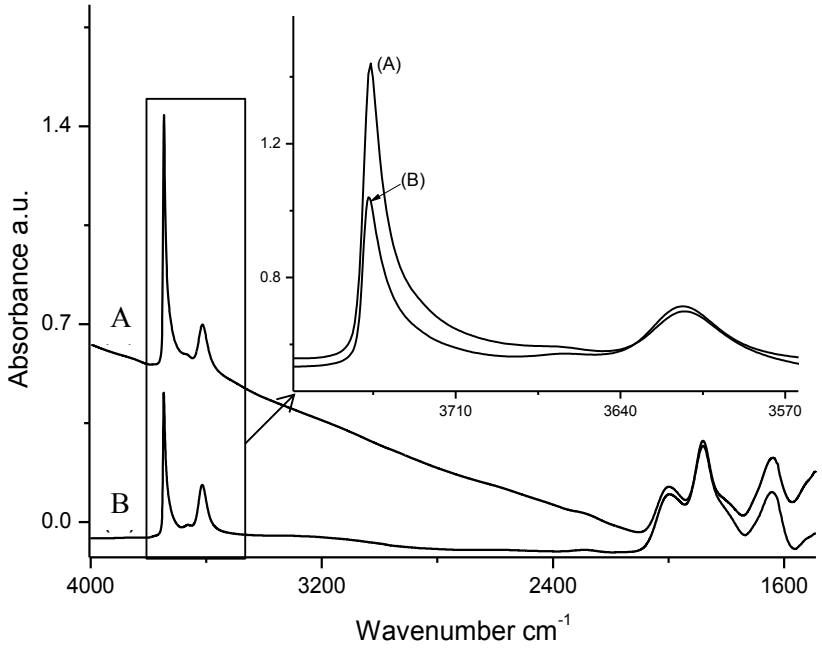

Figure 10. Infrared spectra of activated (A) ZSM-5-OH and (B) ZSM-5-F in the region 4000 -1500 cm^{-1}. Insert: IR spectra of (A) ZSM-5-OH and (B) ZSM-5-F in the OH stretching region.

Brønsted and Lewis sites in the two samples, Pyridine temperature-programmed desorption (TPD) analysis was performed. **Figure 11** shows the infrared spectra of the two samples after adsorption of pyridine. The pyridine's pressure was 1 Torr and the sample was evacuated under vacuum at 523 K. The two samples exhibited similar Brønsted acidity, 0.242 mmol g^{-1} for ZSM-5-OH and 0.236 mmol g^{-1} for ZSM-5-F, but the amount of Lewis sites was different. The calculated Lewis sites in the fluoride medium-synthesized sample was 0.275 mmol g^{-1}, higher than that of ZSM-5-OH (0.213 mmol g^{-1}), which was attributed to larger amount of extra-framework Al species in ZSM-5-F. This result is in agreement with the ^{1}H MAS NMR analysis of the two samples.

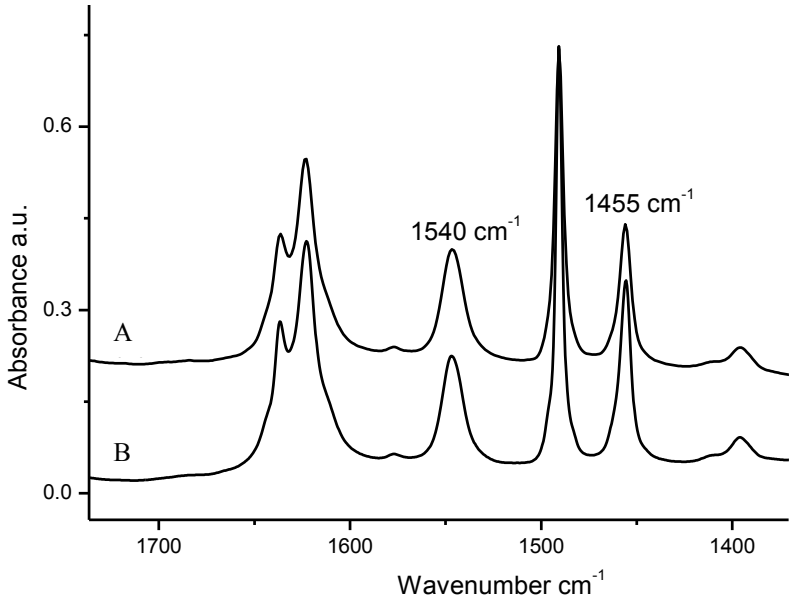

Figure 11. Infrared spectra of (A) ZSM-5-OH and (B) ZSM-5-F after adsorption of pyridine.

2.3 Catalytic tests

Structural defects in zeolites have a direct impact on their catalytic activity and deactivation. A direct correlation between coke formation and silanol defects, during xylene isomerization,

has already been proven by a 2-D IR correlation study.[25] In addition, a recent study showed that the deactivation rate of ZSM-5 during methanol conversion is strongly related to the intensity ratio of the external and internal silanol infrared bands.[23] It was pointed out that the presence of internal defect sites was crucial for the deactivation of the catalysts. In this context, methanol conversion seems to be an ideal reaction to study the catalytic performance of a zeolite synthesized in hydroxyl and fluoride medium.

Figure 12 presents the conversion of methanol versus time on stream for thetwo ZSM-5 catalysts. Although they have similar amount of Brønsted acid sites, the initial activity of ZSM-5-F (80 %) was higher than that of the ZSM-5-OH (70 %). The presence of larger aggregates in the case of ZSM-5-OH and associated diffusion limitations may be the reason for the observed effect. The deactivation rate for two samples was also substantially different. Namely, the deactivation proceeded faster on ZSM-5-OH to reach a 45 % conversion after 106 hours. The methanol conversion over ZSM-5-F after 106 hours on stream was about 67%. This value is equivalent to the conversion reached for the hydroxyl medium-synthesized sample after only 20 hours on the

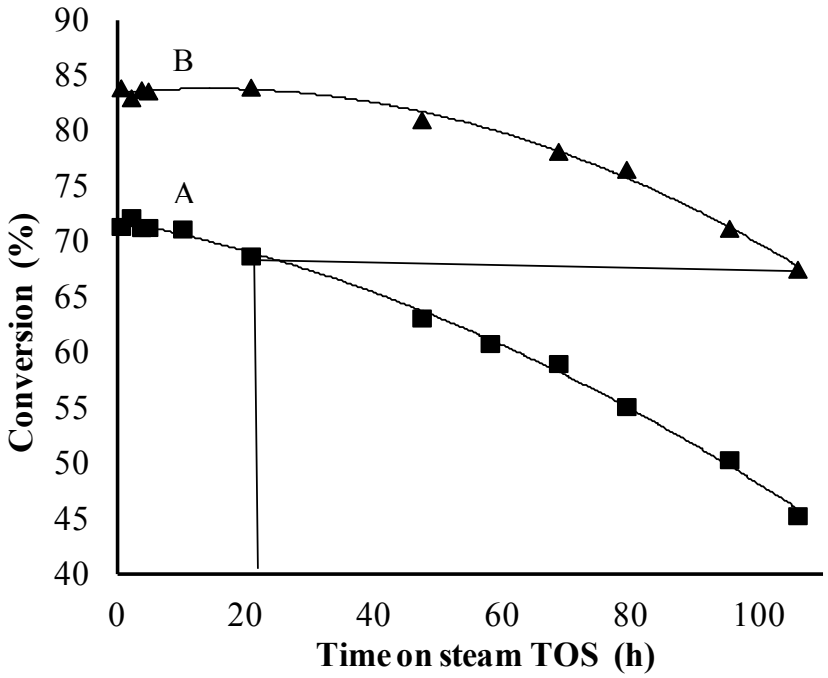

Figure 12. Conversion of methanol into hydrocarbons versus time on stream at 623 K and WHSV = 5.6 g $h^{-1}g^{-1}$ of (A) ZSM -5-OH and (B) ZSM-5-F.

stream. Such a result could be explained by the presence of more structural defects in ZSM-5-OH. As shown by the IR study, ZSM-5-OH displays more silanol defects, which obviously plays an important role in coke formation and catalyst deactivation. As mentioned, a direct correlation between internal silanol defects and coke formation has already been reported in the literature.[23,25]

The product selectivity towards aromatic compounds for both catalysts was around 60 % (**Figure SI7**). The high selectivity towards larger molecules could be related to the shortening of the diffusion pathways in nanosized crystals or to the presence of acidic Lewis sites. As demonstrated in a previous study, desilicated catalysts show higher selectivity towards large molecules due to faster diffusion.[24] In order to determine the key factor for the observed performance of the two catalysts, the total conversion capacity was estimated according to the method usede by Bjorgen et al.[24] The conversion was estimated by plotting methanol conversion as a function of the cumulative methanol converted in grams per gram of catalyst and then extrapolating to zero conversion (**Figure 13**). The total conversion capacity for ZSM-5-OH was found to be equal to 641 g methanol / g of catalyst while that of ZSM-5-F is 1000 g methanol / g catalyst. Thus, when the conversion capacity decreases to 45%, ZSM-5-OH has converted 350 g of methanol per g catalyst while ZSM-5-F has converted about 700 g methanol /g catalyst.

The catalytic data clearly show a better performance of the catalysts synthesized in fluoride medium. ZSM-5-F shows higher initial activity and lower deactivation rate without

substantial changes in the product selectivity.

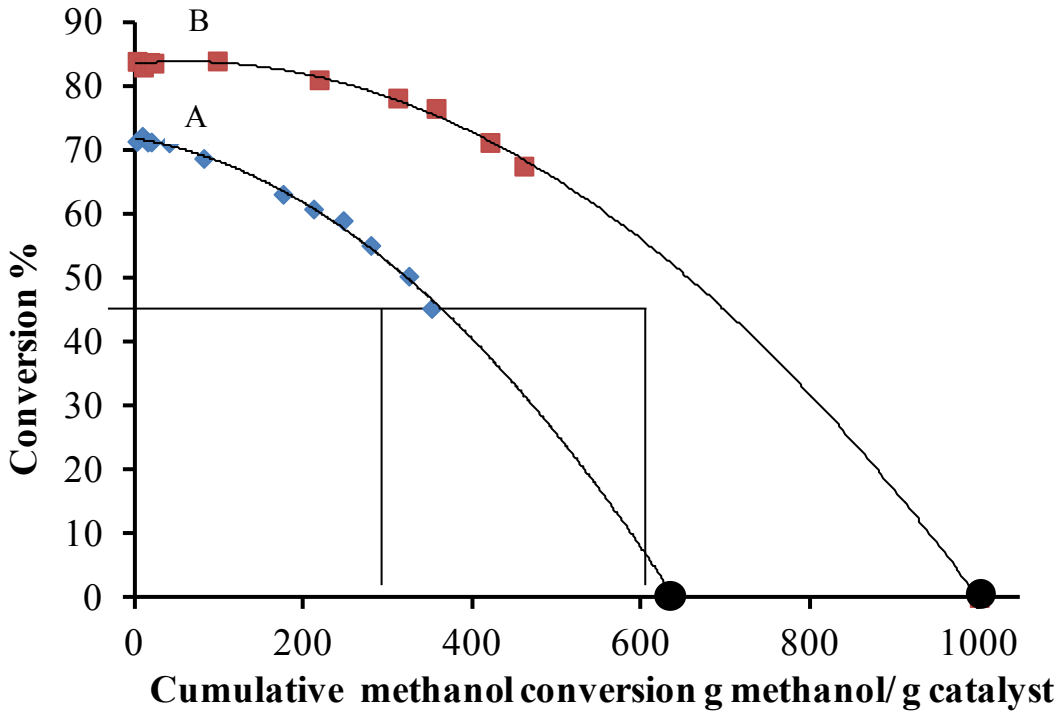

Figure 13. Methanol conversion versus the cumulative amount of methanol converted during reaction for (A) ZSM-5-OH and (B) ZSM-5-F. Extrapolation to zero gives the total conversion capacity of the catalysts; extrapolated points are represented in black circles.

3 Conclusions

ZSM-5 was synthesized in fluoride medium using nanosized silicalite-1 seeds. Syntheses with 2.5, 5.0 and 10.0 wt % seeds were performed. The crystal growth as a function of the seed content was studied. The effect of crystallization temperature on zeolite formation was also studied at 403, 423 and 443 K. These experiments allowed to optimize the ZSM-5 formation in fluoride medium. Highly crystalline products with sizes below 200 nm were obtained. The crystallization time was reduced to 1.5 h at 443 K and 3.5 h at 423 K, respectively. The smallest crystals were synthesized at 403 K. This sample (ZSM-5-F) was employed in a

comparative study of the zeolite characteristics as a function of synthesis medium, as a counterpart nanosized MFI-type sample with similar Si/Al ratio was synthesized in hydroxyl medium (ZSM-5-OH).

The physicochemical characterization of the two ZSM-5 samples was performed employing a set of complementary characterization methods. The similar crystallinity, micropore volume, Si/Al ratio and crystal size allowed to compare their acidic properties and to evaluate in a straightforward manner the effect of synthesis medium on the type, number and distribution of active sites in zeolite catalysts. The two materials exhibited similar number of Brønsted acid sites**.** However, they differed substantially in the surface silanols, as ZSM-5-OH possessed substantially larger number of defect sites. Consequently, hydroxyl medium-synthesized zeolite showed lower catalytic activity and faster deactivation. The superior catalytic performance of ZSM-5-F was attributed to the lower number of defect sites and thus slower deactivation of the catalyst.

The results of this study unambiguously prove that seeded zeolite synthesis in a fluoride medium can be used to decrease the crystal size and thus to circumvent the major disadvantage of zeolite materials synthesized under such conditions.

4 Experimental

4.1 Synthesis of ZSM-5 samples in F- and OH- medium

The following chemicals were used in the synthesis of ZSM-5 samples: aluminum metal powder (99.5 %, Alfa Aesar), tetra-n-propylammonium hydroxide (TPAOH, 20 wt.% water solution, Alfa Aesar), fumed silica (99.8 %, Aldrich), NH_4F (98 %, Aldrich), tetraethyl orthosilicate (TEOS, 98 %, Aldrich), aluminum isopropoxide (98 %, Aldrich), tetrapropylammonium bromide (TPABr, 98 %, Aldrich) and hydrochloric acid (HCl, 37 %, Carlo Erba Reagents). The synthesis of ZSM-5 samples in fluoride medium (F-ZSM-5) was performed from a gel with the composition: 0.142TPABr : 0.135TPAOH : $0.072Al_2O_3$: $1.0SiO_2$: $0.616NH_4F$: $20H_2O$. After mixing the initial reactants, a suspension comprising 0-10 wt % silicalite-1 seeds with respect to the silica content in the gel was added to the mixture. Seed crystals ware prepared according to the procedure described in Ref. 26. The pH of the gel was then adjusted to 8.5 using 0.1 M HCl. The high density of the gel did not allow the use of a pH meter, thus highly accurate pH paper (Merck KGaA) was used for the pH adjustments. The resultant slurry was vigorously stirred for 1 h. The synthesis was performed at 403, 423 and 443 K for different periods of time so as to study the zeolite crystal growth kinetics. The solid product was collected by filtration, washed thoroughly with distilled water and dried at room temperature overnight.

The synthesis of ZSM-5 sample in OH^- medium (OH-ZSM-5) was performed from a gel with the following composition: 0.147TPAOH : $0.0067[(CH_3)_2CHO]_3Al$: 0.2TEOS : $3.507H_2O$. Aluminium isopropoxide $[(CH_3)_2CHO)_3Al]$ was firstly dissolved in TPAOH to obtain clear solution. Then TEOS was added and the resultant mixture was kept at room temperature for 6 h to hydrolyze TEOS. The ethanol formed from the hydrolysis of TEOS was evaporated using a rotary evaporator at 353 K for 45 min. Then the synthesis was performed at 443 K for 120 h. The solid formed was collected by filtration, washed

thoroughly and dried at room temperature overnight.

4.2 Physicochemical characterization

Powder X-ray diffraction (XRD) patterns were obtained with a PANalytical X'Pert Pro diffractometer using Cu Kα radiation (λ = 1.5418 Å, 45 kV, 40 mA). All analyses were performed using ca. 20 mg powder loaded on a silicon wafer. The samples were studied in the 5 - 50° 2θ range with a scanning step of 0.0167 ° s^{-1}. The relative crystallinity was calculated by comparing the diffraction intensities of the five major peaks at 2θ = 23.1, 23.2, 23.6, 23.9 and 24.3 ° to the intensity of the most crystalline sample.

Scanning electron micrographs were taken on a MIRA-LMH (TESCAN) scanning electron microscope (SEM) equipped with a field emission gun.

Nitrogen adsorption measurements were performed with a Micromeritics ASAP 2020 automated gas adsorption analyzer. Prior to analysis, the samples were outgassed 573 K for 12 h. Specific surface areas were determined from the BET equation. The total volume was calculated from the volume adsorbed at P/P_0 = 0.99. The t-plot method was used to distinguish the micropores from the mesopores in the samples and to calculate the external surface areas.

Infrared (IR) spectra were recorded with a Nicolet Magna 550-FT-IR spectrometer at 2 cm^{-1} optical resolution. Prior to IR measurements, the catalysts were pressed into self-supporting discs (diameter: 1.6 cm, 18 mg) and were pretreated in the IR cell attached to a vacuum line at 823 K (2 K /min) for 5 h down to 10^{-6} Torr. The adsorption of pyridine was performed at 373 K. After establishing a pressure of 1 Torr at equilibrium, the cell was evacuated at 523 K in order to remove the physisorbed species. All spectra were normalized to 20 mg wafers. The amount of pyridine adsorbed on Brønsted and Lewis sites was determined using the integrated area of the bands observed at 1545 cm^{-1} and 1454 cm^{-1}, respectively. The extinction

coefficients used in this study were the following: $\varepsilon(B)_{1545}$=1.02 and $\varepsilon(L)_{1454}$=0.89 cm/mol.[27] Solid-state magic angle spinning nuclear magnetic resonance spectroscopy (MAS-NMR) was used to characterize the local ^{29}Si, ^{27}Al, ^{19}F and ^{1}H environments in MFI prepared in OH^- and F^- medium. All data were recorded on a Bruker advance 400 MHZ spectrometer using 4 mm rotor. The ^{29}Si MAS NMR spectra were recorded at 79.4 MHz, a pulse length of 4 μs (30° flip angle), a spinning rate of 14 kHz and a repetition time of 20 s. The ^{27}Al MAS NMR spectra were recorded at 104.3 MHz with a $\pi/12$ pulse length of 2.2 μs, a spinning rate of 14 kHz and a recycle delay of 1 s. ^{19}F was measured at 376.28 MHz, using Hartman-Hann echo with a $\pi/2$ pulse of 7 μs, a spinning rate of 14 kHz and a recycle delay of 5s. Finally, ^{1}H MAS NMR was performed on samples dehydrated at -723 K for 4 h under vacuum. A Hartman-Hann echo was used with a $\pi/2$ pulse of 3.5 μs, a spinning rate of 14 kHz and a recycle delay of 2 s. TMS was used as reference for chemical shifts of ^{1}H and ^{29}Si, $Al(NO_3)_3$ (1 M) for ^{27}Al and $CFCl_3$ for ^{19}F.

Elemental analysis was performed by inductively coupled plasma–atomic emission spectroscopy (ICP-AES) using an OPTIMA 4300 DV (Perkin–Elmer) instrument.

4.3 Catalytic tests

MTH reaction tests were performed at 623 K in a fixed bed quartz reactor using 20 mg of catalyst. The reaction temperature was controlled via a thermocouple inserted in the reactor. Catalysts were activated, prior to reaction, at 723 K for 4 hours at a heating rate of 1.6 K/min under air flow (50 $mlmin^{-1}$). Then a nitrogen flow, 20 $mlmin^{-1}$, saturated with methanol (99.6 %) via a bubble saturator was introduced in the reactor. The saturator temperature (283 K) was controlled by a constant temperature bath. The methanol feed rate was estimated to 7.2 % from the gas flow rate and the saturated vapour pressure (WHSV=5.6 g. h-1/g of catalyst). The reactor effluents were analysed by an online gas

chromatograph (GC Varian 3900; Column WCOT fused silica CP wax 52 CB 0.32 μm). To avoid condensation, the connecting lines between reactor, saturator and GC were heated to 343 K. It is noteworthy that dimethyl ether was considered as reactant and added to methanol amount in the calculation of conversion and selectivity.

ACKNOWLEDGEMENTS

The authors acknowledge the French National Scientific foundation (Agence Nationale de la Recherche - ANR) for the financial support of this work (ANR 2010 BLAN 723 1). Dr. Lakiss acknowledges the Lower Normandy Region for her research grant.

References

[1] D. Breck, *Zeolite Molecular Sieves*, John Wiley&Sons, New York, 1974.

[2] A. Corma, *Chem. Rev.* **1995**, *95*, 559.

[3] V. Valtchev, G. Majano, S. Mintova, J. Perez-Ramirez, *Chem. Soc. Rev.* **2013**, *42*, 263.

[4] S. Mintova, V. Valtchev, *Microporous Mesoporous Mater.* **2002**, *55*, 171.

[5] C. Cundy, P. Cox, *Microporous Mesoporous Mater.* **2005**, *82*, 1.

[6] E. M. Flanigen, R. L. Patton, US Patent 4073865, 1978.

[7] J.-L. Guth, H. Kessler, J. M. Higel, J. M. Lamblin, J. Patarin, A. Seive, J. M. Chezeau, R. Wey, *ACS Symp. Ser.* **1989**, *398*, 176.

[8] V. Valtchev, S. Mintova, *Encyclopedia of Inorganic Chemistry*, C. M. Lukehart & R. A. Scott (Eds.), John Wiley & Sons, Chichester, Ch. ia380, pp 543-562, 2008.

[9] C. Fyfe, D. H. Brouwer, A. R. Lewis, J.-M. Chezeau, *J. Am. Chem. Soc.* **2001**, *123*, 6882.

[10] E. Aubert, F. Porcher, M. Souhassou, V. Petricek, C. Lacomte, *J. Phys. Chem. B* **2002**, *106*, 1110.

[11] H. Koller, A. Wölker, L. A. Villaescusa, M. J. Diaz-Cabanas, S. Valencia, M. A. Camblor, *J. Am. Chem. Soc.* **1999**, *121*, 3368.

[12] A. Pulido, A. Corma, G. Sastre, *J. Phys. Chem. B* **2006**, *110*, 23951.

[13] (a) G. Sastre, J. A. Vidal-Moya, T. Blasco, J. Rius, J. L. Jorda, M. T. Navaro, F. rey, A. Corma, *Angew. Chem. Int. Ed.* **2002**, *41*, 4722; (b) A. Corma, M. Puche, F. Rey, G. Sankar, S. Teat, *Angew. Chem. Int. Ed.* **2003**, *42*, 1156.

[14] (a) M. Alvaro, P. Atienzar, A. Corma, B. Ferrer, H. Garcia, M. T. Navarro, *J. Phys. Chem. B* **2005**, *109*, 3696 ; (b) A. Corma, M. J. Diaz-Cabanas, J. Martinez-Triguero, F. Rey, J. Rius, *Nature* **2002**, *418*, 514; (c) R. Castaneda, A. Corma,V. Fornes, F. Rey, J. Rius, *J.*

Am. Chem. Soc. **2003**, *125*, 7820; (d) A. Corma, M. J. Diaz-Cabanas, F. Rey, US Patent 6797254, 2003. (e) A. Corma, M. J. Diaz-Cabanas, J. L. Jorda, C. Martinez, M. Moliner, *Nature* **2006**, *443*, 842.

[15] S. Ivanova, C. Lebrun, E. Vanhaecke, C. Phan-Huu, B. Louis, *J. Catal.* **2009**, *265*, 1.

[16] U. Olsbye, S. Svelle, M. Bjorgen, P. Beato, T. V. W. Janssens, F. Joensen, S. Bordiga, K. P. Lillerud, *Angew. Chem. Int. Ed.* **2012**, *51*, 2.

[17] G. Majano, A. Darwiche, S.Mintova, V. Valtchev, *Ind. Eng.Chem. Res.* **2009**, *48*, 7084.

[18] S.K. Sur, R.G. Bryant, *Zeolites* **1996**, *16*, 118.

[19] H. M. Kao, Y.-C. Chen, *J. Phys. Chem. B* **2003**, *107*, 3367.

[20] M. Gaillard, V. Montouillout, F. Mauge, C. Fernandez, *Stud. Surf. Sci. Catal.* **2004**, *154*, 1679.

[21] H. Jon, Y. Oumi, K. Itabashi, T. Sano, *J. Cryst. Growth* **2007**, *307*, 177.

[22] G. Engelhardt, D. Michel. *High-Resolution Solid State NMR of Silicates and Zeolites*, John Wiley & Sons, Chichester, 1987.

[23] K. Barbera, F. Bonino, S. Bordiga, T.V.W. Janssens, P. Beato, *J. Catal.* **2011**, *280*, 196.

[24] M. Bjorgen, F. Joensen, M. S. Holm, U. Olsbye, K. P. Lillerud, S. Svelle, *Appl. Catal. A: General* **2008**, *345*, 43.

[25] F. Thibault-Starzyk, A. Vimont, Ch. Fernandez, J.-P. Gilson, *Chem. Commun.* **2000**, 1003.

[26] L. Tosheva, V. P. Valtchev, *Chem. Mater.* **2005**, *17*, 2494.

[27] N. Nesterenko, F. Thibault-Starzyk, V. Montouilliout, V. Yushchenko, C. Fernandez, J.-P. Gilson, F. Fajula, I. Ivanova, *Kinet. Catal*. **2006**, *47*, 40.

TOC

The study reports the synthesis of nanosized ZSM-5 crystals in fluoride medium. A set of complementary characterization methods is used to compare the intrinsic characteristics of nanocrystals obtained in fluoride medium with those of counterpart nanocrystals obtained in hydroxyl medium. The catalytic performance of materials in methanol conversion is studied and the results related to the effect of synthesis conditions on zeolite properties.

Keywords: zeolite; nanocrystals, fluoride medium synthesis, catalysis

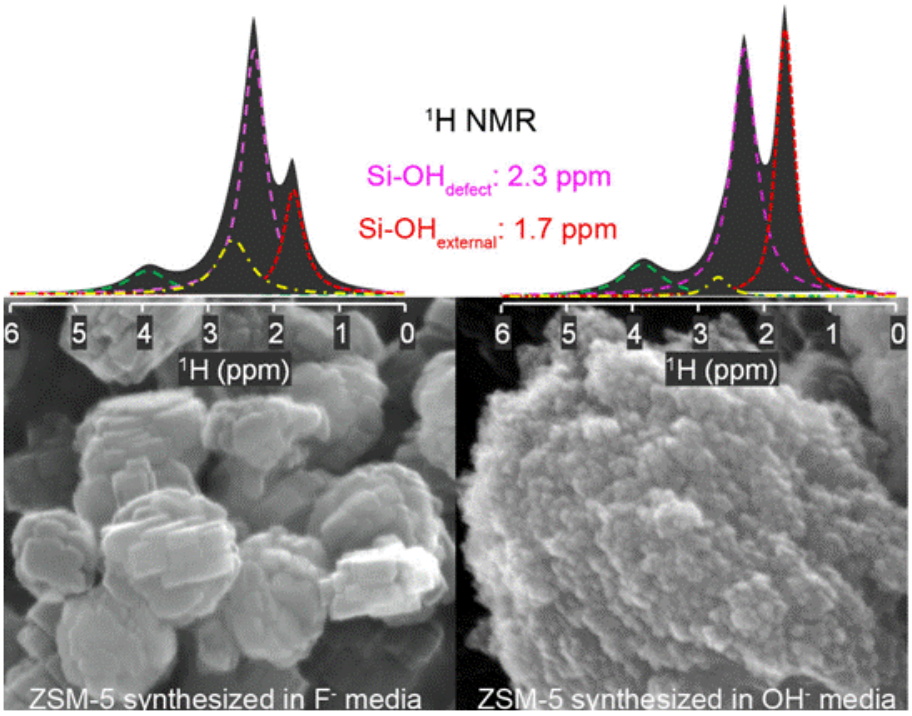

The study reports the synthesis of nanosized ZSM-5 crystals in fluoride medium. Their intrinsic characteristics are compared with those of counterpart nanocrystals obtained in a hydroxyl medium. The catalytic performance of the two materials in methanol conversion is studied and the results are related to the effect of the synthesis conditions on the zeolite properties.

Supporting Information

Comparative study of nano-ZSM-5 catalysts synthesized in OH^- and F^- medium

Zhengxing Qin,[a] Louwanda Lakiss,[a] Lubomira Tosheva,[b] Jean-Pierre Gilson,[a] Aurelie Vicente,[a] Christian Fernandez,[a] Valentin Valtchev[a*]

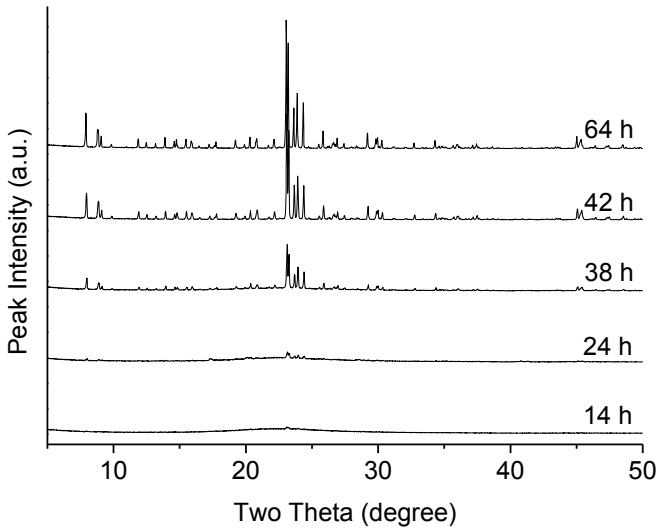

Figure SI1. XRD patterns of the samples synthesized from a seeds-free system at 423 K for different periods of time.

.

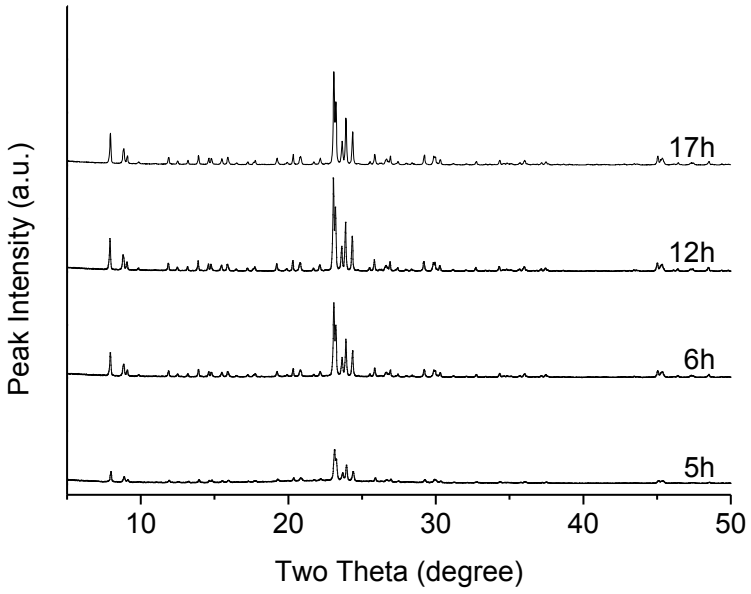

Figure SI2. XRD patterns of the samples synthesized at 423 K for different periods of time from a system comprising 2.5 wt. % silicalite-1 seeds.

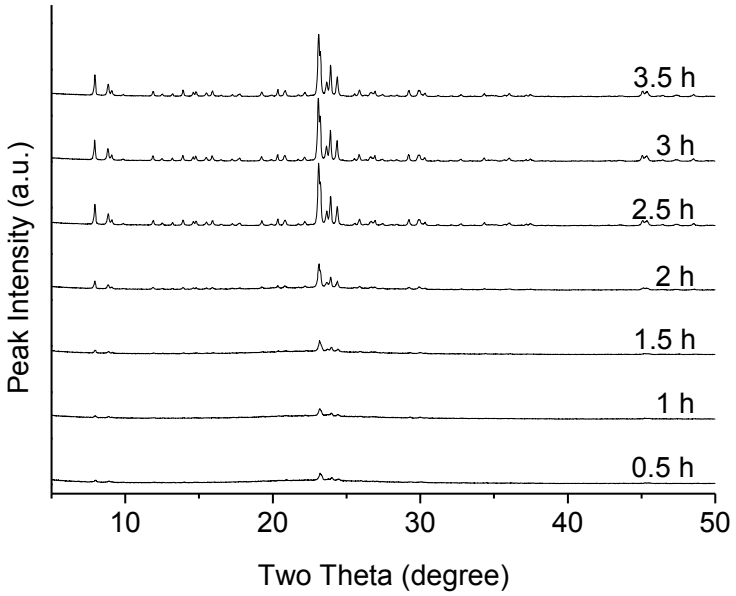

Figure SI3. XRD patterns of the samples synthesized at 423 K for different periods of time from a gel comprising 5 wt. % seeds.

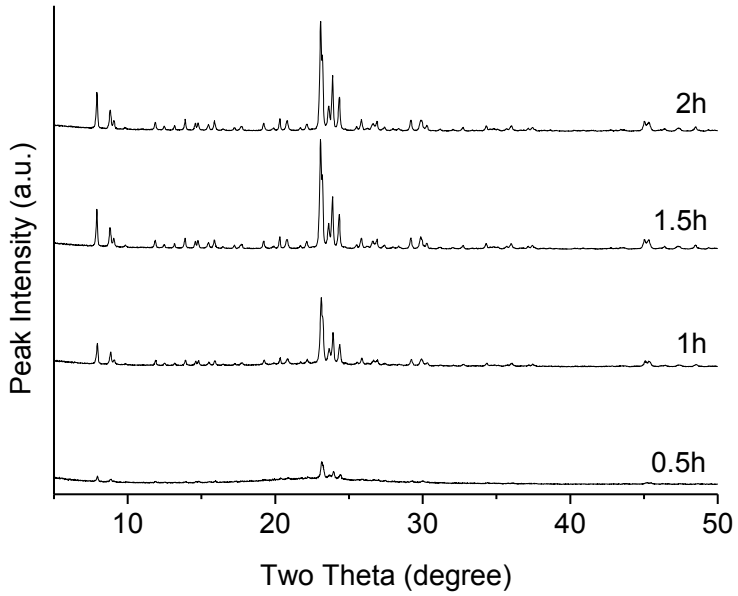

Figure SI4. XRD patterns of the samples synthesized at 443 K at the presence of 5 wt.% seeds.

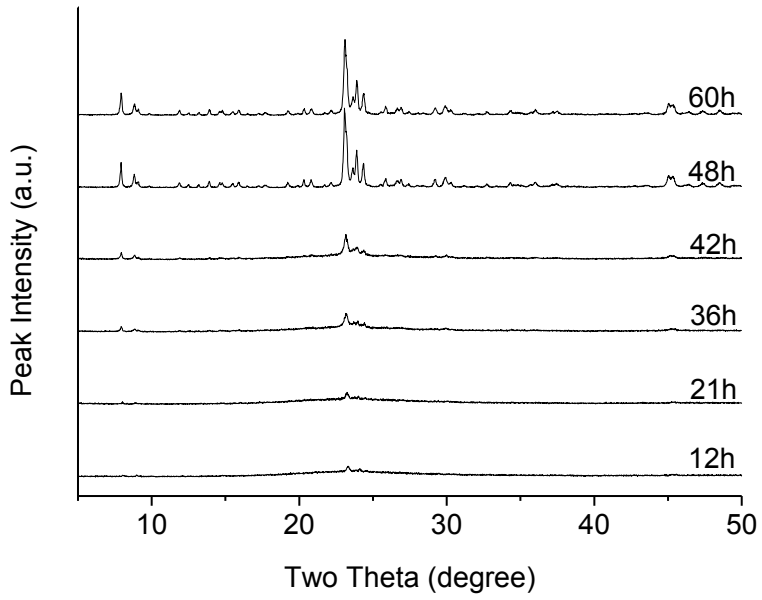

Figure SI5. XRD patterns of the samples synthesized at 403 K at the presence of 5 wt.% seeds.

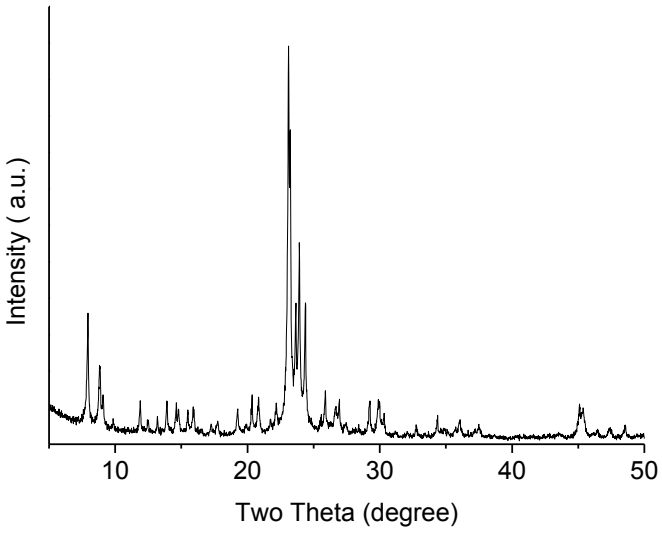

Figure SI6. The XRD pattern of the nano-ZSM-5 zeolite synthesized in OH^- medium.

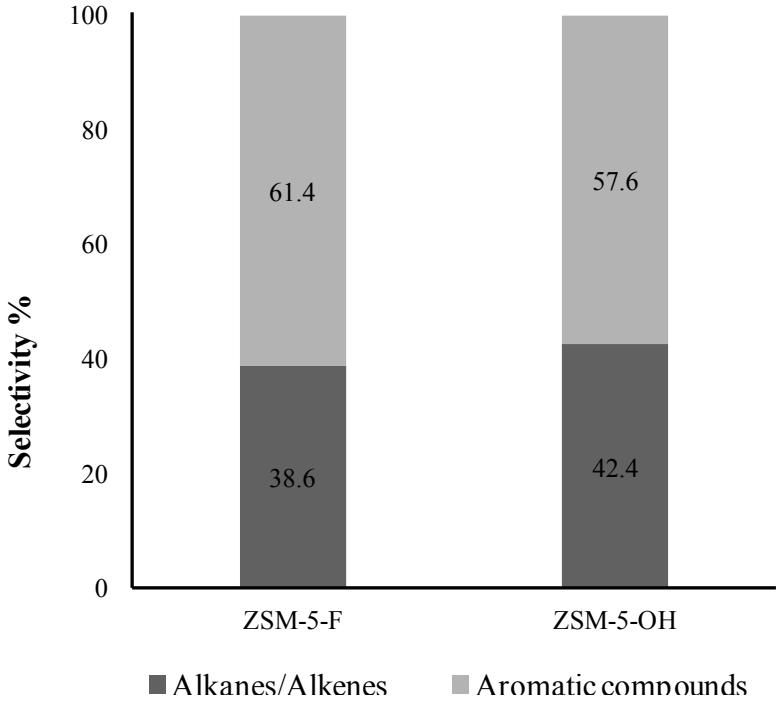

Figure SI7. Product selectivity of ZSM-5-F and ZSM-5-F during methanol conversion.